LA-12776-MS
c.3

LA-12776-MS

Prototype Explosives-Detection System Based on Nuclear-Resonance Absorption in Nitrogen

REPRODUCTION
COPY
IS-4 REPORT SECTION

LOS ALAMOS NATIONAL LABORATORY
3 9338 00296 5258

Los Alamos
NATIONAL LABORATORY

Los Alamos National Laboratory is operated by the University of California for the United States Department of Energy under contract W-7405-ENG-36.

Edited by Robert Graybill, Technical Communication Services, for Group CIC-1
Illustrations by AnnMarie Dyson, Group CIC-1
Composition and layout by Randi Bagley, Group CIC-1

This work was supported by the Federal Aviation Administration.

An Affirmative Action/Equal Opportunity Employer

This report was prepared as an account of work sponsored by an agency of the United States Government. Neither The Regents of the University of California, the United States Government nor any agency thereof, nor any of their employees, makes any warranty, express or implied, or assumes any legal liability or responsibility for the accuracy, completeness, or usefulness of any information, apparatus, product, or process disclosed, or represents that its use would not infringe privately owned rights. Reference herein to any specific commercial product, process, or service by trade name, trademark, manufacturer, or otherwise, does not necessarily constitute or imply its endorsement, recommendation, or favoring by The Regents of the University of California, the United States Government, or any agency thereof. The views and opinions of authors expressed herein do not necessarily state or reflect those of The Regents of the University of California, the United States Government, or any agency thereof.

LA-12776-MS

UC-000
Issued: June 1994

Prototype Explosives-Detection System Based on Nuclear-Resonance Absorption in Nitrogen

R. E. Morgado
G. Arnone
C. C. Cappiello
S. D. Gardner
C. L. Hollas
L. E. Ussery
J. M. White
J. D. Zahrt
*R. A. Krauss**

**Federal Aviation Administration, Atlantic City International Airport, NJ 08045*

LOS ALAMOS NATL. LAB. LIBS.
3 9338 00296 5258

Los Alamos
NATIONAL LABORATORY
Los Alamos, New Mexico 87545

Contents

PROTOTYPE EXPLOSIVES-DETECTION SYSTEM BASED ON NUCLEAR-RESONANCE ABSORPTION IN NITROGEN

by

R. E. Morgado, G. Arnone, C. C. Cappiello, S. D. Gardner,
C. L. Hollas, L. E. Ussery, J. M. White, J. D. Zahrt, and R. A. Krauss

ABSTRACT

A protoype explosives-detection system (EDS) that was developed for experimental evaluation of a nuclear-resonance absorption technique is described. The major subsystems are a proton accelerator and beam transport, high-temperature proton target, an airline-luggage tomographic inspection station, and an image-processing/detection-alarm subsystem. The detection system performance, based on a limited experimental test, is reported.

---

1. INTRODUCTION AND BACKGROUND

The development of the pre-prototype explosives-detection system described here is based on an earlier feasibility study[1] completed in 1989 in which the detection of nitrogen in an explosive simulant was demonstrated by scanning it with a gamma-ray beam of an energy corresponding to a nuclear resonance in nitrogen.[2] Our earlier study also suggested that, by this technique, certain explosives should be distinguishable from inert materials commonly encountered in airline-passenger luggage.

Scaling from these results, we projected that a very-high-current (≈5 mA) proton accelerator, which is used to generate the resonant-energy gamma rays, would be needed to meet the Federal Aviation Administration's (FAA's) 6-s/bag throughput requirement. The developmental efforts described here were originally envisioned to include the development of this high-current accelerator for a fully operational, semi-automated prototype detection system for test and evaluation in an airport. However, due to budget constraints, the scope of the project was scaled back to that of a laboratory test of a reduced-throughput, nonautomated system. Thus, some of the major subsystems that have been developed incorporate some of the design features of an airport prototype—the detector, data acquisition, and image-processing subsystems—while the accelerator and related subsystems are for a reduced throughput (by an order of magnitude). Nevertheless, this pre-prototype system permits evaluation of many of the important operational characteristics of an airport system, which is the principal objective of the project.

In this report, the physical basis of the detection concept will be presented, followed by a description of each major subsystem and its key performance characteristics. We will also present some results of our initial explosives-detection tests, from which preliminary conclusions on overall system performance are drawn.

This FAA-sponsored project was a collaborative effort of the Los Alamos National Laboratory (LANL) and the Soreq Nuclear Research Center (SNRC) of Yavne, Israel. Two variants of the detector/luggage-inspection system were pursued by the respective collaborators, but each used a common accelerator/gamma-ray production system. The following report addresses only the LANL detection approach. .

2. PHYSICAL BASIS OF THE DETECTION CONCEPT

The strong resonance photoproton cross section of nitrogen, $^{14}N(\gamma,p)^{13}C$, is described by the Breit-Wigner equation,

$$\sigma\left(E_\gamma\right)=\frac{\Pi\lambda^2 g\Gamma_\gamma\Gamma_p}{\left(E_\gamma-E_R\right)^2+\left(\frac{\Gamma}{2}\right)^2}, \qquad (1)$$

where:

$$\lambda=h\frac{c}{E\gamma}=21.5\ \text{fm}$$
$$\Gamma_\gamma=7\ \text{eV}$$
$$E_R=9.17\ \text{MeV}$$
$$\Gamma_p=115\ \text{eV}$$
$$g=2J+\frac{1}{2(2I+1)}=\frac{5}{6}$$
$$\Gamma=122\ \text{eV}.$$

The cross section for nitrogen near the 9.17-MeV resonance[3-5] is shown in Fig. 1.

The extreme narrowness of this peak in the resonance, while representing a unique signature for nitrogen, presents a serious practical problem in generating an adequate resonant-energy gamma-ray flux to make this technique useful. After briefly investigating filtered bremsstrahlung sources, which we found to have adverse signal-to-noise ratios, we adopted the $^{13}C(p,\gamma)^{14}N$ reaction[6] (the inverse to resonance absorption) as the preferred gamma-ray source. The proton source for this reaction dictates the use of a particle accelerator, and the practicality of the approach depends largely on achieving sufficiently high proton currents from the accelerator.

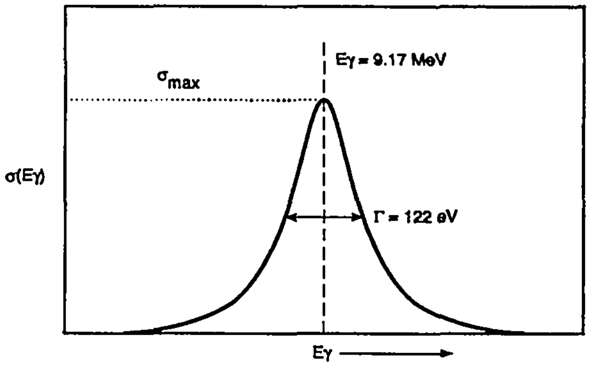

Fig. 1. ^{14}N nuclear-resonance absorption cross section.

Because of the Doppler shift from the recoiling ^{14}N in the above reaction, only those gamma rays emitted in an ≈0.7-degree-wide beam at 80.7 degrees from the direction of the proton beam (in the laboratory frame of reference) are at the precise resonance energy. Thus, the locus of resonant photons is a narrow 80.7-degree conical section whose axis coincides with the proton beam.

The transmission of a resonant energy beam through a volume containing both nitrogen and other material is given by

$$T_R=\frac{I_R}{I_0}=\exp\left[-\left(f\sigma_R+\sigma_{NR}\right)\Delta m\right], \qquad (2)$$

where the total cross section is the sum of resonance cross section, σ_R, and that for the nonresonant processes, σ_{NR}; f is the mass fraction of nitrogen; and Δm the total mass thickness in atoms/cm^2. The nonresonant attenuation,

$$T_{NR} = \frac{I_{NR}}{I_0} = \exp\left(-\sigma_{NR}\Delta m\right), \qquad (3)$$

can be determined independently from simultaneous off-resonance measurements of gamma-ray transmission. Thus, the nitrogen mass thickness is

$$\Delta N = f\Delta m = \frac{1}{\sigma_R}\ln\left(\frac{T_{NR}}{T_R}\right). \qquad (4)$$

The off-resonance measurement is done by including barium fluoride in the ^{13}C target, which produces 6.13-, 6.9-, and 7.1-MeV gamma rays from the (p,αγ) reaction in ^{19}F. Transmission measurements at these energies can be extrapolated to the resonant energy with sufficient accuracy to determine the nonresonant contribution to the total cross section. Transmission measurements through liquid nitrogen were used in determining the effective σ_R for the actual measurement system. A schematic of the detection concept is shown in Fig 2.

3. OVERALL DESCRIPTION OF THE PROTOTYPE DETECTION SYSTEM

Figure 3 shows the physical layout of the principal subsystems of the detection system. The accelerator produces a horizontal, pulsed beam of 1.75-MeV protons, which pass through a focusing quadrupole and beam energy debuncher, and are turned downward by a combination bending and focusing magnet to produce a ≈1-cm-diam beam spot on the ^{13}C target. The resultant conical fan beam of gamma rays is approximately (within 10 degrees) horizontal. Luggage is positioned onto the surface of a platform that incrementally rotates 360 degrees to produce multiple views of a slice of the luggage. The luggage platform is raised or lowered by a constant increment (the "slice" thickness) between the successive rotational scans, until the vertical cross section of the bag has been scanned.

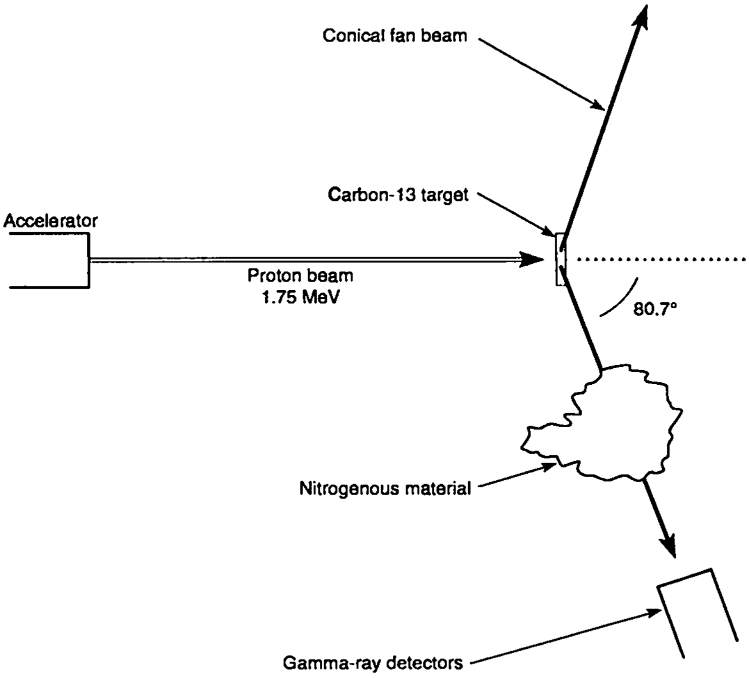

Fig. 2. Resonance-absorption-based detection concept.

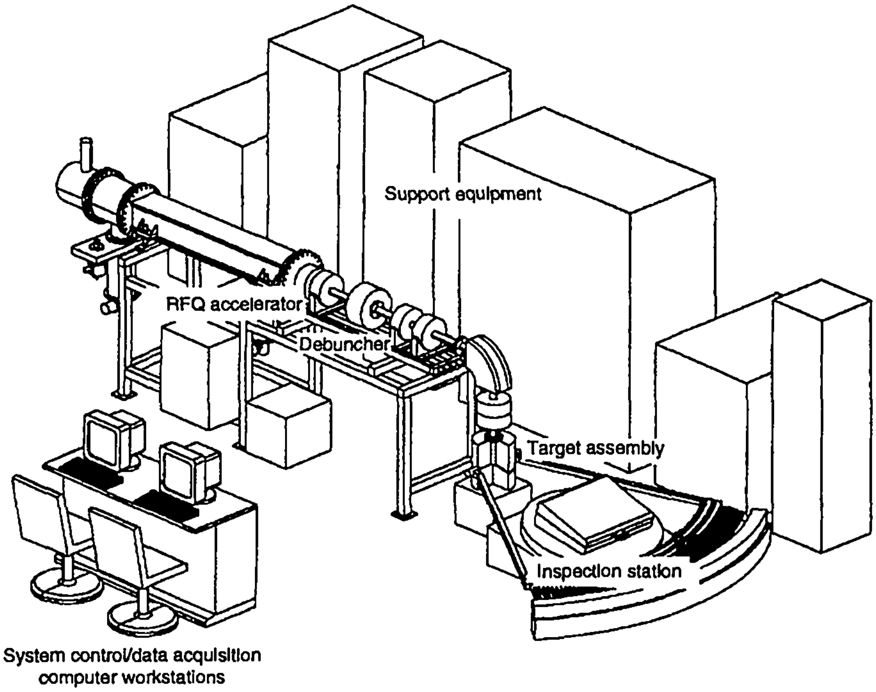

Fig. 3. Physical configuration of the detection system.

An array of gamma-ray detectors is positioned on the locus of the resonant-energy beam and spans approximately one quadrant of the fan beam. Individual detector outputs are collected, preprocessed, and transmitted to a computer workstation and temporarily stored in the data acquisition workstation. Upon completion of a luggage inspection, the data are transmitted to a second computer workstation for a tomographic reconstruction showing the luggage contents.

Two images of the contents are produced: one from the nonresonant (6- and 7-MeV) gamma rays, which provides a 3-D image of the mass distribution within the inspection volume, and another of the nitrogen distribution using the resonant, 9.17-MeV gamma rays. Although they are not automated at this stage of development, a number of image-processing techniques are available to ascertain the likelihood of the presence of explosives.

A more detailed description of each of these major subsystems is given below.

4. PROTON ACCELERATOR

The proton accelerator used for this project was a radio-frequency quadrupole (RFQ) linac acquired by Los Alamos and modified and partially upgraded by the FAA for resonance-absorption applications. One objective of the project was to evaluate the suitability for resonance-transmission measurements of an RFQ linac (pulsed beam) in comparison with electrostatic accelerators (CW beam). The principal issue centers on the beam characteristics typical of an RFQ accelerator, e.g., the effect of beam emittance (energy and geometric) and the micro- and macro-structure of the pulsed beam on transmission measurements. Other considerations are inherent beam stability, size, cost, etc. (These issues, as well as a detailed description of the accelerator and associated beam-transport system, are discussed in detail in Ref. [7].)

5. PROTON TARGET

The most prominent design issue regarding the proton target is its ability to withstand the heat load imposed by the high-current proton beam. The original design requirement was for a 5-mA beam. This was subsequently relaxed to a 0.5-1.0-mA beam, although the targets used in these tests incorporated some of the features for the higher power levels. Other design considerations included the minimization of unwanted secondary gamma-ray production in the copper backing and ease of fabrication.

The first-generation designs were for power densities of ≤ 4 kW/cm^2. A water-cooled copper backing was used to dissipate the heat. The water was transported through channels machined into the back of the target to within 1.6 mm of its front face. These channels took the form of a logarithmic spiral (see Fig. 4), which produced a turbulent radial flow away from the central hot spot. Several coating variants were fabricated (see Table I) and tested. Excitation curves and gamma-ray spectra were obtained for a sample from each batch as a check on the thickness of deposited materials.

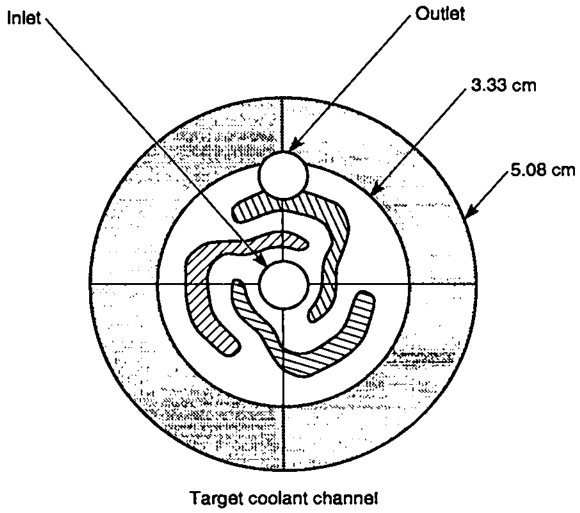

Fig. 4. High-power target design.

The Set # 1 duplicates our earliest design, which was first tested in 1991 at power levels of ≤ 1 kW/cm^2 at the University of Birmingham (UK) Dynamitron CW accelerator. In the others, the ^{13}C thickness was increased to accommodate the inherent proton energy spread (estimated to be ≥ 20 keV) associated with the accelerating process (bunching) of an RFQ accelerator. The purpose of the hafnium was to facilitate interlayer bonding. The layer of gold was necessary to degrade the proton energy to that of the fluorine resonance level; and, in Set #3, the tantalum further degraded the proton energy to ≤ 500 keV, so that the gamma-ray background induced by the copper would be markedly lower. The coatings were applied by vapor deposition with a four-hearth electron-beam source. A quartz crystal monitor was employed to control coating thicknesses. The final thicknesses and coating

Table I. Thick target coatings.

Target Set	Layer	Material	Thickness
#1	1	Carbon 13	148 μg/cm^2
	2	Hafnium	300 Å
	3	Gold	5750 Å
	4	Hafnium	300 Å
	5	Barium fluoride	1300 Å
	6	Hafnium	300 Å
#2	1	Carbon 13	160 μg/cm^2
	2	Hafnium	500 Å
	3	Barium fluoride	1300 Å
	4	Hafnium	300 Å
#3	1	Carbon 13	176 μg/cm^2
	2	Hafnium	300 Å
	3	Gold	5750 Å
	4	Hafnium	300 Å
	5	Barium fluoride	1300 Å
	6	Tantulum	10 μm

densities were determined from either profilometer measurements of witness plates or from microbalance differential weights.

No degradation of these targets was detected in the course of operational testing of the detection system; however, the heat loading was only moderate (generally less than 2 kW over a period of ≤ 200 h).

6. LUGGAGE MANIPULATOR

The luggage manipulator (see Fig. 5) sequentially positions vertically and orients rotationally the luggage in the resonant-energy beam to obtain the different viewing directions required for tomographic image reconstruction. For each vertical position, the luggage manipulator table rotates the bag in uniform increments through 360 degrees. Upon completion of a rotational viewing sequence, the platform is raised or lowered by an amount determined by the beam width. This viewing sequence is repeated until the entire bag thickness is scanned. In these tests, either 32 or 64 viewing directions were employed. The slightly diverging beam was approximately 1.8-cm wide at the center of rotation of the turntable.

The manipulator table is capable of rotating and elevating luggage having a maximum lateral dimension of 91 cm (36 in.) and a maximum vertical dimension of 41 cm (16 in.). It is driven by stepping motors with shaft encoders that indicate the position of the table. The platform is mounted on an elevator that is driven by a ball-screw/ball-nut on each corner of the platform. The four ball nuts are driven by a single stepping motor through drive belts. Ball bushings on guide shafts guide the elevator, which is mounted on a tilt wedge for precise alignment of the manipulator platform with the beam direction.

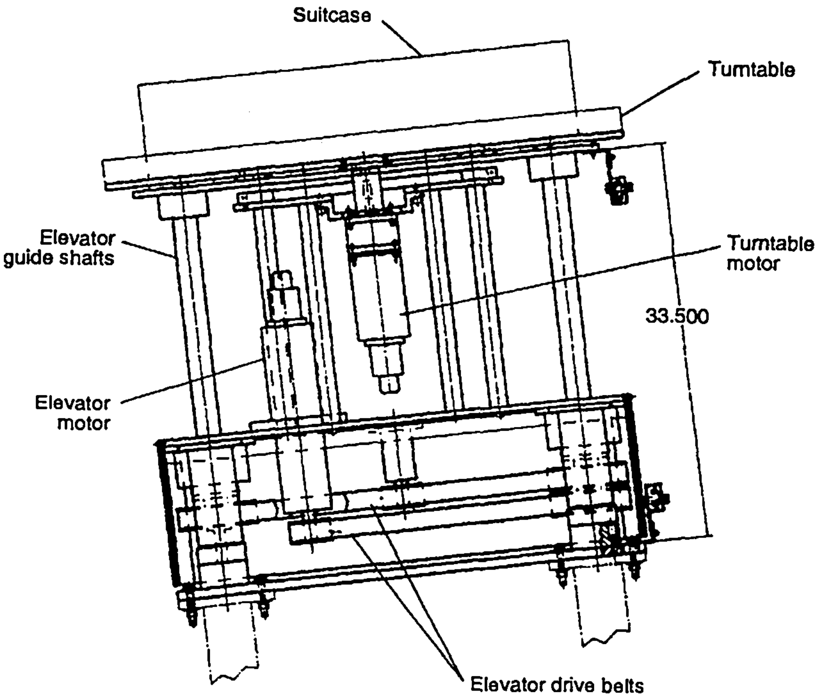

Fig. 5. Luggage manipulator.

The motion of the manipulator is controlled digitally from the data acquisition computer workstation. The number of rotational views and the viewing slice thickness are selectable by the operator. The duration of each view is determined by the number of recorded gamma-ray counts; each view is continued until the desired number of counts is obtained. The desired counting statistics are also selected by the operator.

7. GAMMA-RAY DETECTOR SYSTEM

Selecting the optimum dimensions for individual gamma-ray detectors is a difficult trade-off between opposing factors: maximum spatial resolution requires small detectors, while maximum efficiency dictates larger detector crystals. Another consideration in the design process is the nature of the scintillator material, which affects efficiency, spectral resolution, and stability. Finally, the optical coupling of the scintillator crystal to the photomultiplier tube (PMT) can also materially affect performance. The design process for determining the best combination of detector parameters was iterative, involving extensive computer modeling of detector response and experimental tests of different scintillator materials, geometries, and PMT coupling approaches.

Bismuth germinate (BGO) was chosen as the baseline scintillator material on the basis of its high stopping power (high Z), adequate spectral resolution (sufficient to resolve the 6- and 7-MeV resonance lines and the 9.17-MeV ^{14}N resonance), and stability. However, it does require auxiliary temperature stabilization. We chose a detector diameter of 3 cm, which is the minimum size for an acceptable detector efficiency. The detector slit width was ≈2 cm, as dictated by the angular width of the resonance photon beam. The resultant average pixel size was ≈2.0 cm x 1.3 cm. The 3-D spatial resolution of the viewing system is a function of these dimensions and the number of tomographic viewing directions.

Several approaches for PMT optical coupling were investigated, but the most acceptable required tapering the crystal to match the aperture of the PMT. The resultant crystal geometry is shown in Fig. 6. The custom-designed detectors were supplied by the Bicron Corporation. Sixty-four detector assemblies were required in order to span the lateral dimension of the specified inspection volume. The measured energy resolution of the detectors averaged ≈15%.

The detector mounts, beam collimator, and support stand were designed as an integral structure to support and align the BGO detectors and provide a 10-cm-thick lead collimator slit. Figure 7 illustrates the assembled support system. Vitreous carbon spacers maintained the collimator slit spacing. Chilled-water lines were attached to the upper aluminum cover plate of the detector mounts to stabilize the scintillator crystal temperature at 17°C.

8. DATA ACQUISITION SYSTEM

The data acquisition system receives the signal output of the 64 detectors; processes and categorizes the data according to detector location, inspection slice, and viewing direction; and stores the data for transfer to the tomographic-image-processing system. It also provides the necessary hardware and software to control and monitor the luggage-inspection platform-motion equipment, accelerator, and high-voltage supplies. The general design guidelines were

1. provide near-real-time output (i.e., a process rate of $\approx 1.6 \times 10^6$ events/s),
2. minimize dead-time contribution, and
3. use commercial hardware and software whenever possible.

The selected system was VMEbus-based and used VxWorks (Wind River Systems) as the real-time operating system. The VMEbus protocol permits 21 or more CPUs per crate. All software development was done on a Sun SPARC II workstation, which permits convenient

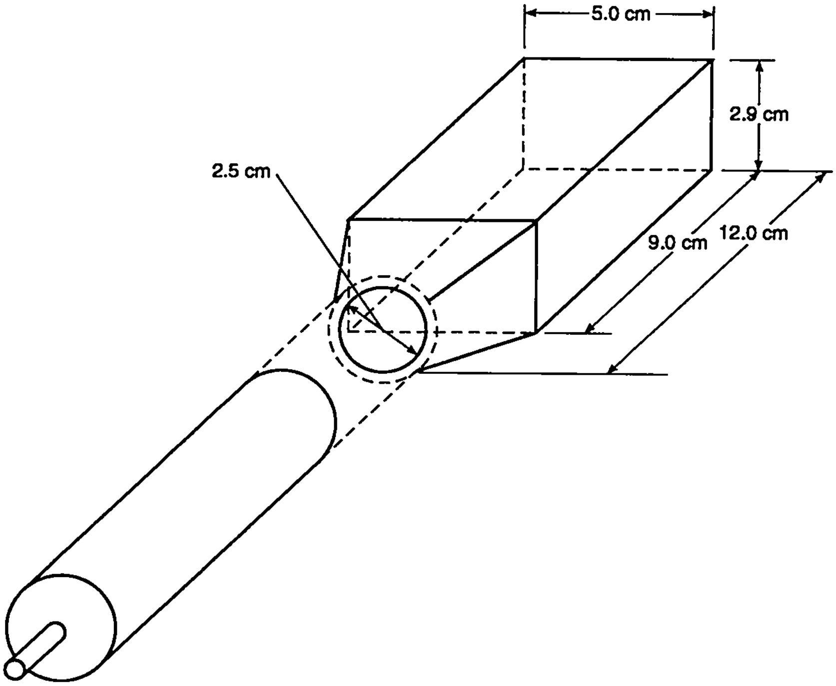

Fig. 6. Tapered BGO crystal and light pipe.

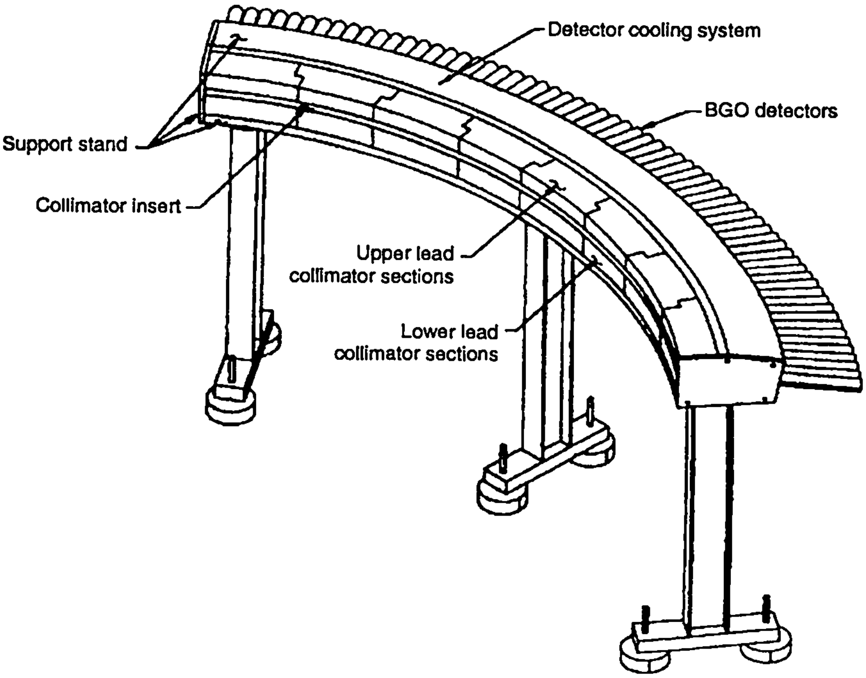

Fig. 7. Collimated detector array.

downloading of software to each CPU as executable code.

The detector signals feed the VMEMCA board (Fig. 8), which comprises two sections: a commercial, 3U-sized, 68030 CPU with dual-ported memory, PROMS, serial I/O, etc., and a daughter-board interface that allows custom boards to be attached; and a custom-designed analog processing section with 12 independent channels, each containing a low-level discriminator (LLD), programmable gain amplifier (PGA), charge integrator, analog-to-digital converter (ADC), and a first-in first-out memory (FIFO).

When an input pulse from the gamma-ray detector exceeds the LLD threshold, the charge integrator constructs a delayed version of the pulse. The integration time is software-selectable from 100 ns to 12 ms (a minimum of 400 ns is used, in keeping with the bismuth germinate decay time of 300 ns). After charge integration, the signal is digitized by the ADC and stored in the FIFO. The dead-time contribution, not including integration time, is < 100 ns. The program executed by VMEMCA's CPU sequentially reads each FIFO of the analog section, which is tagged with the detector ID and the luggage-platform vertical and rotational position, and provides the memory address used in constructing an energy histogram and a region-of-interest display. For a 125-kHz single-channel instantaneous rate, the dead time ranges from 6% to 16%. Tests showed the system will adequately resolve our multi-energy spectra for all anticipated operating conditions.

9. TOMOGRAPHIC IMAGE PROCESSING

A tomographic approach was chosen for analyzing the resonance transmission measurements because, in principle, it can provide a detailed 3-D mapping of the nitrogen-density distribution within the luggage. This generally is necessary for analyzing irregularly shaped explosives devices. As noted above, transmission measurements are also made at off-resonance energies, from which the mass distribution within the luggage can be obtained as well. Although the nitrogen density alone can be a reliable signature, the combination of nitrogen density and total density clearly improves the accuracy of material identification, especially for cases involving marginal counting statistics.

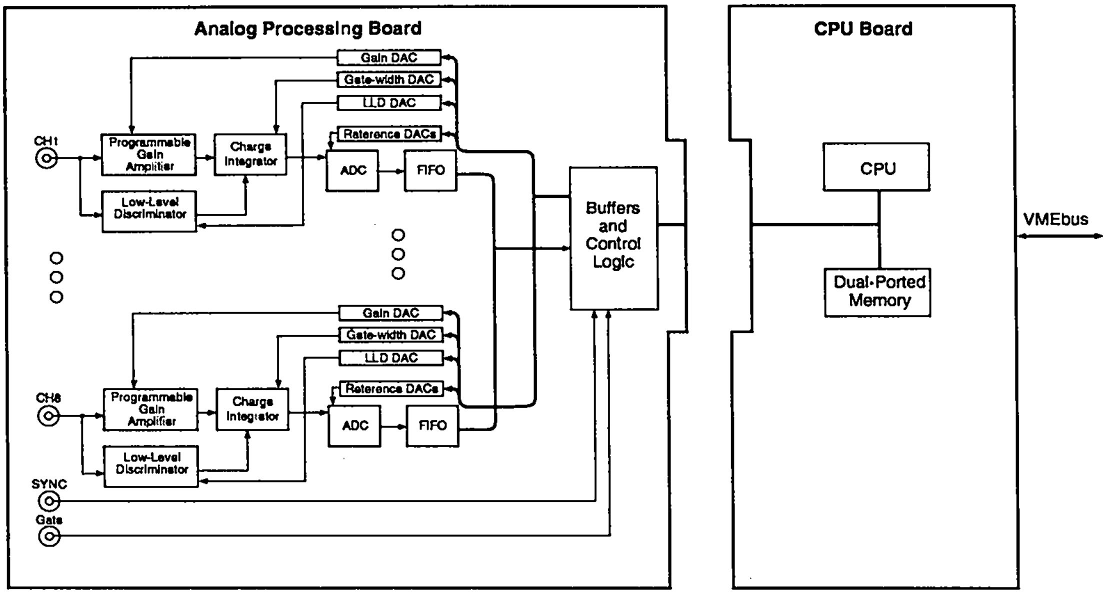

Fig. 8. VMEMCA block diagram.

The image processing is built around KHOROS, a fully developed, public-domain code (University of New Mexico) for information processing, data visualization, and software development. KHOROS also allows the inclusion of special-purpose routines developed by the user. A number of these routines have been written for this project, although some are not yet used at this early stage of testing. (The tomographic reconstruction software is incorporated into KHOROS as a special-purpose routine.)

At the current stage of development, the tomographic algorithm reconstructs a cross-sectional 2-D image of each slice. These are convenient for visual (nonautomated) interpretation of the images. The cross-sectional images can be displayed sequentially and, from interslice comparisons, the vertical locations of objects can be established. Although an initial version of a 3-D image reconstruction algorithm has been completed and partially tested, it has not been integrated into the system.

As indicated earlier, images are reconstructed of both the total-density distribution and the nitrogen-density distribution ("nitrograms"). The shape of higher-density objects generally can be determined from the nonresonance image. Any objects with density outside the expected range for explosives ($\approx$1.0-1.9 g/cm^3) are inferred not to be explosives. Objects with densities within the explosives range are compared to the nitrogram image, and if the nitogram indicates a significant nitrogen density at the corresponding location, the object is presumed to be an explosive. (Automation of the preceding simple alarm protocol, and others under consideration, is not anticipated until an extensive image data base is available for evaluation and optimization of the system.)

10. INITIAL DETECTION EXPERIMENTS

Because of programmatic time constraints, detectability testing of the EDS using live explosives began immediately upon completion of system assembly. Thus, the tests reported below are a part of the preliminary system optimization experiments and do not represent the expected capabilities of the system. Nevertheless, they provide an indication of the system's performance potential.

A blind-test system-detectability demonstration was conducted by an FAA-led explosives-handling team. The team, in collaboration with explosives-development organizations at Los Alamos, independently acquired for these tests a range of explosives that differed by type, density, mass, nitrogen content, and shape. Selected explosives were placed in FAA-supplied (unclaimed) luggage at a remote magazine and delivered by this team to the experimental site. The individual bags were placed on the inspection table for each test, monitored during the luggage-inspection period, and then returned to a holding area. Knowledge of the luggage contents was restricted to the FAA team. The blind-test protocol provided for an extended period of time following this test series before the experimental team had to declare the detection results. This period permitted some software debugging, system calibration, etc., that normally would have taken place prior to the demonstration. After the detection results are declared, the FAA team will reveal the actual contents of the luggage to the experimental team.

A total of 14 bags were inspected in these blind tests (the majority containing explosives but some with explosives simulants), but the declared results of these tests are not yet available. However, results of a system-calibration test can be reported. It was carried out in the same manner as the other tests but used a piece of luggage that contained known explosives and simulants. Although a very limited test, it provides an indication of the minimum potential capabilities of the technique.

Figure 9 shows a sketch of the calibration bag, its explosives contents, and the operational test parameters. The system-calibration bag was prepared by the FAA team and contains specimens representing four explosive types (see Table II) and geometries that range in total mass

Table II. Test Explosives Physical Properties (nominal values).

Name	Principal Constituents	Density (g/cm^3)	^{14}N Density (g/cm^3)
Deta Sheet D	75% PETN	1.48	0.19
Baratol	TNT/Ba(NO$_3$)$_2$	2.63	0.39
9205 PBX	92% RDX	1.71	0.59
Deta Sheet C	63% PETN	1.48	0.23
Composition B Simulant	—	1.60	0.47

from 2/3 to 1-1/2 of a "threat quantity" of explosive. (The "threat quantity" represents the minimum amount of that particular explosive that the system was designed to detect.)

The explosive sheets are representative of the geometric extremes for practical explosive devices and, for this calibration test, were oriented approximately perpendicular and parallel to the viewing direction.

As noted before, the image-processing system constructs a tomographic image of the cross section of the bag for each viewing slice. Image reconstructions of two of the slices near the top of the bag are shown in Fig. 10, which illustrates the detection capabilities and limitations of the unop-

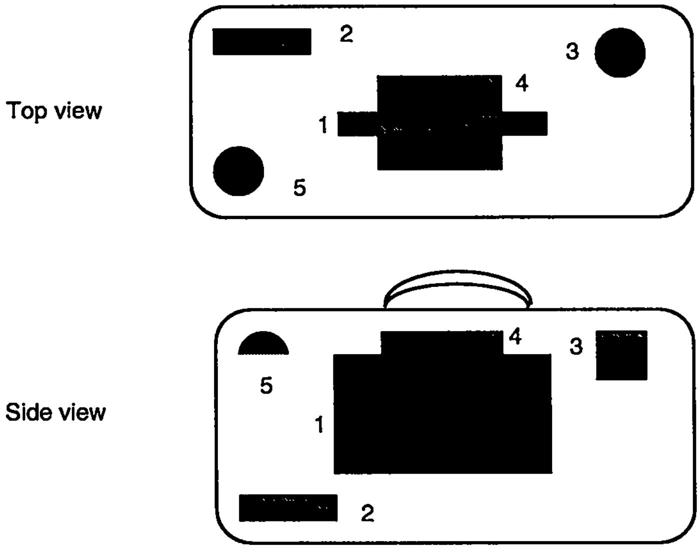

Inspection Parameters

Views:	64
Slice thickness:	1.2 cm
Counts/view:	400
Slices:	6
Bag contents:	Clothes

Test Explosives

1. DETA Sheet C, 6-mm thick, 1.09 x threat
2. Baratol, 2-in. cyl., 1.18 x threat
3. 9205 PBX, 2-in.cyl., 1.48 x threat
4. DETA Sheet D, 5-mm thick, 1.07 x threat
5. Comp. B Sim., hemisphere, 0.65 x threat

Fig. 9. Calibration-bag test parameters.

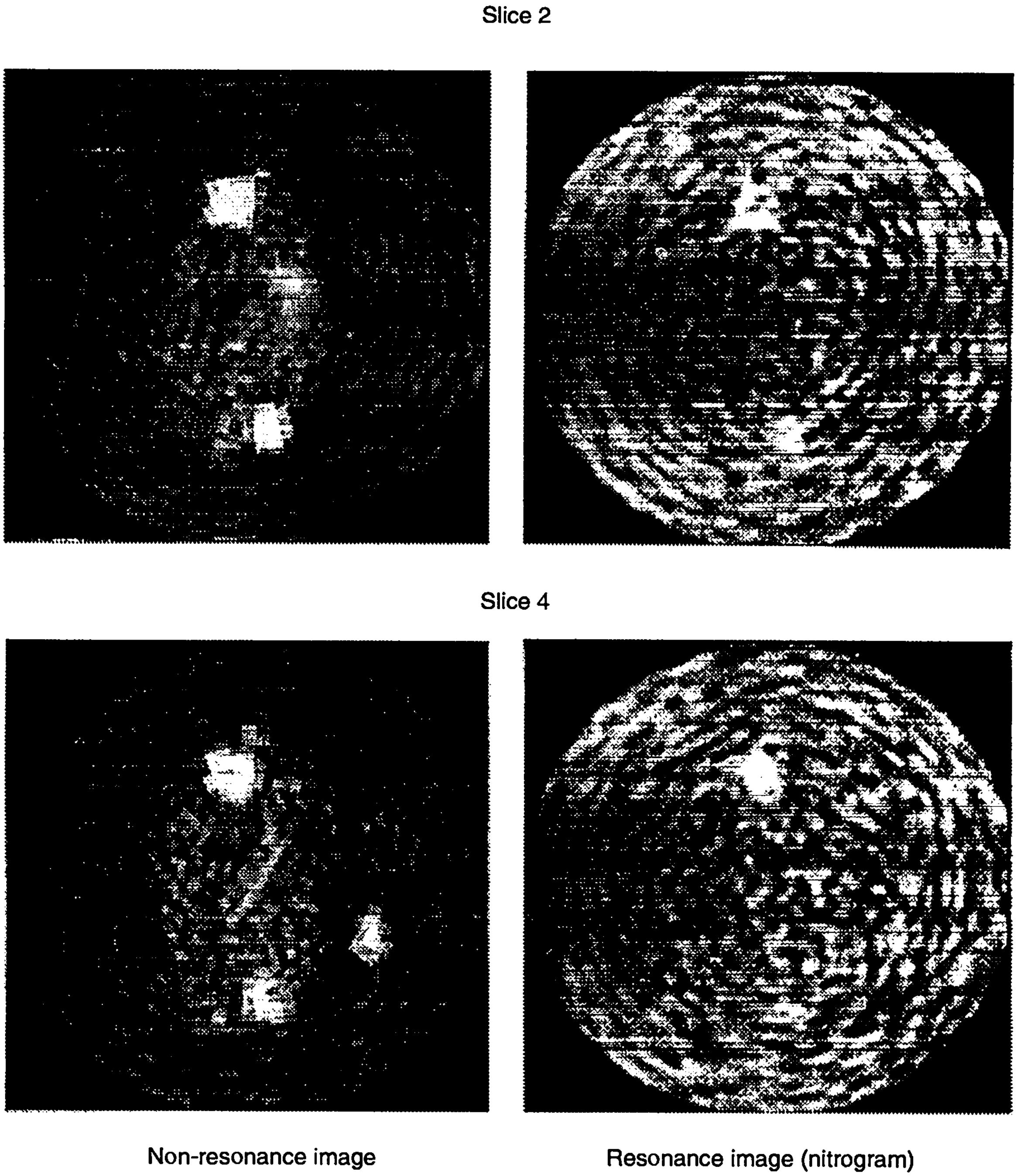

Fig. 10. Image reconstructions of the calibration bag.

timized system in these first tests. The image pairs are from the nonresonance (left) and resonance (right) transmission measurements. The viewing perspective is from above the bag, loking downward (i.e., the top view in Fig. 9). It shows the density distribution over two selected horizontal cross sections (slices) of the bag. (In these reconstruction displays, the longitudinal axis of the bag is rotated clockwise approximately 45 degrees from the top of the page.)

Slice 2 is ~3 cm below the top of the bag, and at this level intersects with test objects #3, #4, and #5 (see Fig. 9, side view). The upper, high-density object (bright area) in the reconstructions is the 9205 PBX (#3 in Fig. 9, seen in both slices) and the lower object is a hemispherically shaped Composition B simulant (#5 in Fig. 9). The horizontal sheet explosive (#4) was not precisely parallel to the plane of the beam, and slice 2 intersects only about 1/3 of the sheet. In the left-hand reconstruction of slice 2, the diffuse, brighter region between and slightly to the right of test objects #3 and #5 is the portion of the sheet explosive (#4) noted above. The nitrogram of slice 2 clearly indicates the presence of high-density nitrogen in #3 and #5, but not for the sheet explosive (#4). However visual comparisons of successive slices in the original images marginally suggest the presence of nitrogen.

In slice 4 (~5 cm below the top of the bag), the beam still intersects test objects #3 and #5, but now the vertical sheet (#1) has come into view. In the lower-right quadrant of the reconstruction, a calibration standard positioned just outside the bag also has come into view. The vertical sheet (aligned with the longitudinal axis of the bag) can also be seen near the center of the nonresonance reconstruction.

In part, a 3-D tomographic approach was included in the system-design concept to determine whether it would significantly improve detectability in the case of sheet explosives. However, 3-D imagery, and the associated special image-processing techniques, are yet to be applied. Another known deficiency in the tested detection system is associated with the unoptimized beam transport system, which, because of an improperly focused proton beam, caused a reduction in the effective nitrogen cross section, which would also contribute to a lower apparent nitrogen density.

11. CONCLUSIONS

We conclude from this very limited test that a detection system based on this approach should readily detect nitrogen explosives in amounts well below our design objective, especially if they are in a compact geometry. We expect significant improvements from various system optimization measures and from the use of 3-D reconstructions. As these initial results suggest, these improvements will be necessary for detecting low-nitrogen-content explosives and sheet explosives. However, the actual detectability limits of this approach—as well as the very important issue of false alarms—cannot be addressed until system optimization is complete and an appropriate statistical data base acquired.

12. REFERENCES

1. "The Feasibility of Detecting FAA-Threat Quantities of Explosives in Luggage and Cargo Using Nuclear Resonance Absorption in Nitrogen, Phase I Final Report," Los Alamos National Laboratory, Advanced Nuclear Technology, internal report (October 1989).
2. M. B. Goldberg, D. Vartsky, et al., Informal Proposal, Soreq Nuclear Research Center, Yavne, Israel, December 1985.
3. S. S. Hannah and L. Meyer-Schutzmeister, "Resonant Absorption by the 9.17-MeV Level in ^{14}N," *Physical Review* **115**, 4 (1959).
4. W. Biesiot and P. B. Smith, "Parameters of the 9.17-MeV Level in ^{14}N," *Physical Review C* **24**, 6 (1981).
5. D. Vartsky, M. B. Goldberg, G. Engler, A. Goldschmidt, A. Breskin, R. E. Morgado, C. L., Hollas, L. E., Ussery, B. L., Berman, and C. E. Moss, "The Total Width of the 9.17-MeV Level in ^{14}N," *Nuclear Physics* **A505** pp. 328-336 (1989).
6. J. D. Seagrave, "Radiative Capture of Protons by ^{13}C," *Physical Review* **85**, 2 (1952).
7. R. E. Morgado, C. C. Cappiello, M. P. Dugan, et al., "The Effects of Proton-Beam Quality on the Production of Gamma Rays for Nuclear Resonance Absorption in Nitrogen," Los Alamos National Laboratory document LA-UR-93-3588 (October 1993).

* U.S. GOVERNMENT PRINTING OFFICE 1994-0-573-024 / 7012

This report has been reproduced from the
best available copy.

It is available to DOE and DOE contractors from the
Office of Scientific and Technical Information,
P.O. Box 62,
Oak Ridge, TN 37831.
Prices are available from
(615) 576-8401.

It is available to the public from the
National Technical Information Service,
US Department of Commerce,
5285 Port Royal Rd.,
Springfield, VA 22161.

LOS ALAMOS NAT'L LAB.
IS-4 REPORT SECTION
RECEIVED

'94 JUL 19 PM 12 56

Los Alamos
NATIONAL LABORATORY
Los Alamos, New Mexico 87545